PVTx Measurements of the *N*-Methylpyrrolidone/Methanol Mixed Solvent: Cubic and SAFT EOS Analyses

Santiago Aparicio, Begoña García, Rafael Alcalde, María J. Dávila, and José M. Leal*

Universidad de Burgos, Departamento de Química, 09001 Burgos, Spain

Received: January 9, 2006; In Final Form: February 13, 2006

The *PVTx* behavior for the *x N*-methylpyrrolidone (NMP) + (1 − *x*) methanol compressed liquid solvent is reported over the full composition range and within wide pressure and temperature ranges. The derived excess properties were analyzed in terms of structural effects and intermolecular interactions and revealed strong H-bonding heteroassociations between the two components. The cubic equations of state by Soave (SRK), Peng−Robinson (PR), Patel−Teja (PT), and Sako−Wu−Prausnitz (SWP), and the statistical associating fluid theory (SAFT) equation of state, combined with a number of selected mixing rules, were used to correlate and predict the behavior of both the pure components and mixed solvent. While the classical cubic equations of state were not successful in describing the properties of this system, the SWP equation of state and the SAFT yielded reasonably good results.

Introduction

Over the past decades, the modeling of processes has received a great deal of attention as a reliable tool to attain efficient, clean, and optimal new technologies.[1] The increasing development of process design, under the pressure of the growing of chemical and related industries, seeks to create environmentally friendly and low energy consuming conditions. Such modeling is critically dependent on the accurate knowledge of the thermodynamic behavior of the chemicals involved; therefore, the availability of suitable methods and the disposal of reliable physical property data are basic requirements to achieve a proper design.[2,3] Among the thermophysical properties needed for modeling solvent mixtures, *PVTx* data measured under particular conditions (and the several derived thermodynamic properties as well) are key; for instance, the design of industrial plants, pipelines, and pumping systems is based on accurate *PVTx* data of the fluids involved.[4]

On the other hand, knowledge of the pressure and temperature effects on the volume of complex fluid systems, either pure or mixed, is also required both for theoretical thermodynamics calculations and in engineering processes. However, despite the critical role played by *PVTx* data, so far the evaluation of such measurements over wide ranges of pressure, temperature, and composition often is not feasible because of economical and/or time-consuming requirements; hence, the modeling of *PVTx* data constitutes an alternative approach to the problem, in such a way that the modern process simulators include a variety of predictive models. Quite an useful description of the *PVTx* behavior of fluid mixtures involves use of the so-called equations of state (EOS); although these models must be considered with great care to leave out misleading predictions and subsequent errors,[3] such EOS have become powerful tools for the representation of *PVTx* properties over wide ranges of pressure and temperature.

Liquid solvents play an important role in a number of chemical applications.[5] The choice of the proper solvent for a particular process primarily relies on the availability of physical properties.[6] *N*-Methylpyrrolidone (NMP), a low volatile, highly polar, thermically and chemically stable solvent, is fully miscible with water and most organic solvents. NMP is a tertiary, dipolar, nonprotogenic, highly selective amide, used as an inert solvent. Due to its ability to modify the reactivity of reacting states in electron and proton transfer reactions, NMP is widely used in settings such as solvent-reactivity relationships and constitutes quite a simple model molecule for the behavior of rigid, nonassociating polar species. NMP is assumed to be associated by dipole−dipole interactions, the high resulting polarity ($\mu_{30°C}$ = 4.09 D)[7] being attributed to the strong stability facilitated by the planarity of the five-membered ring. The favorable and unique toxicological and environmental properties convert NMP into an ideal candidate to replace advantageously chlorinated solvents.[8] NMP, either pure or mixed, is widely used in chemical engineering,[9] extractive distillation,[10] absorption,[11] gas desulfurization,[12] and coal extraction.[13] Pyrrolidones arouse interest in molecular biology as model molecules for the simulation of more complex systems such as peptides.[14,15]

Over the past years our group has conducted a systematic study on the thermophysical properties of NMP-containing mixtures, both at atmospheric[16−18] and high[19] pressures. To properly analyze the selectivity and capability of NMP, the research performed on the *PVT* behavior of the NMP/water binary mixture[19] is extended in this work to the NMP/methanol mixed solvent over the full composition range, between 278.15 and 358.15 K and pressures up to 60 MPa. In addition, the experimental readings have enabled to calculate isobaric thermal expansivities, isothermal compressibilities, internal pressures, and excess properties. These macroscopic properties have been analyzed in terms of microscopic effects and intermolecular interactions, mainly hydrogen bonding.

The experimental data were correlated with a semiempirical equation and a number of EOS. Since the pioneering work by van der Waals, a huge number of reasonably accurate EOS have been put forward with a variable degree of success.[20] In this work two different types of EOS were selected; because of the easy handling and the relatively accurate results they provide,

* Corresponding author. E-mail: jmleal@ubu.es.

10.1021/jp060143t CCC: $33.50
Published on Web 03/11/2006

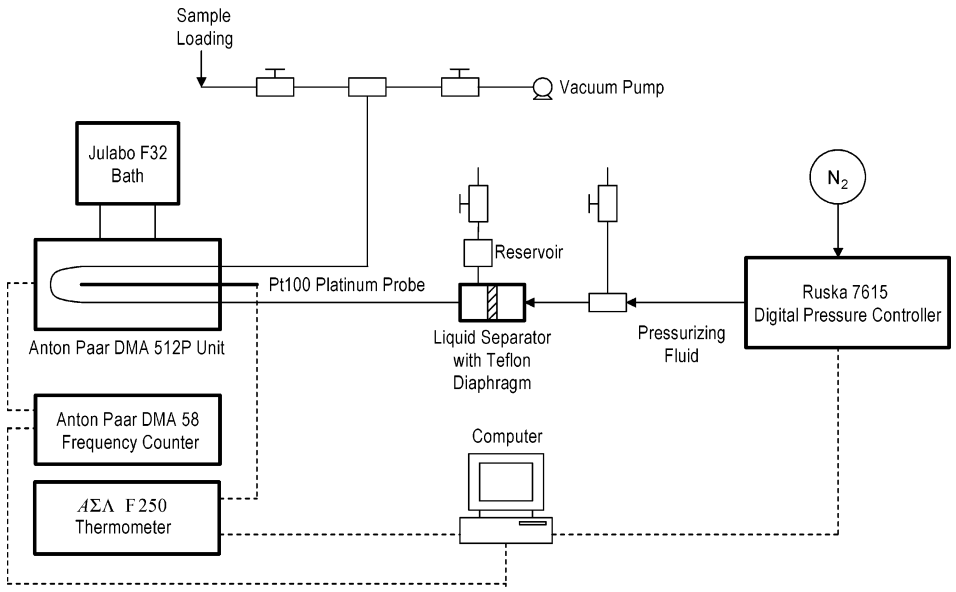

Figure 1. Diagram of the high-pressure density measurement unit. Continuous lines represent hydraulic connections, dashed lines represent electrical connections.

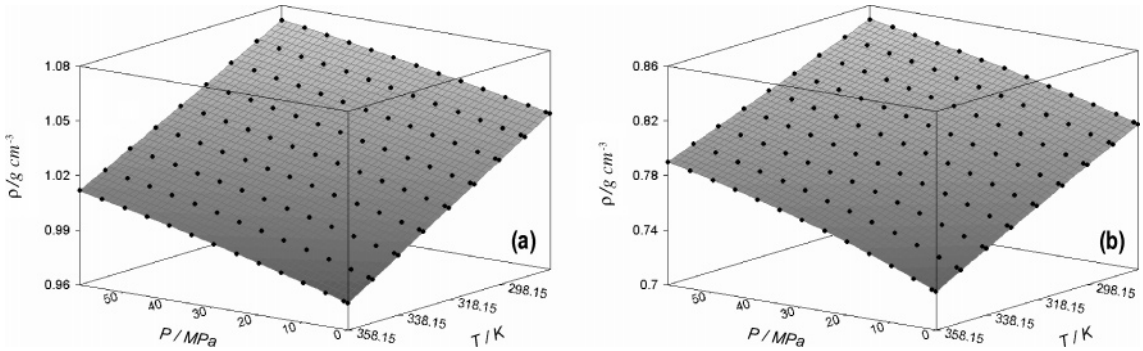

Figure 2. Three-dimensional plot of densities as a function of pressure and temperature for (a) NMP and (b) methanol. (●) Experimental values; the shaded surface obtained with eqs 1−3 and parameters from Table 1.

the cubic EOS (derived from the van der Waals approach) are most used both in the thermodynamic literature and in process design;[21] hence, they play a major role in the modeling of fluid behavior and in the development of fluid state theories as well, the latter being motivated by industrial needs for process design. Thus, to correlate the *PVTx* data of the studied system, the cubic EOS by Soave (SRK),[22] Peng−Robinson (PR),[23] the Stryjek−Vera modification of Peng−Robinson (PRSV),[24] Patel−Teja (PT),[25] and Sako−Wu−Prausnitz (SWP)[26] were used combined with different mixing rules.

This notwithstanding, despite their popularity, cubic EOS are prone to some severe disadvantages, including an inaccurate representation of fluid properties over wide ranges of pressure and temperature;[21] hence, molecularly based EOS constitute a suitable alternative to the classical cubic EOS. In this work, the statistical associating fluid theory (SAFT)[27,28] based on Wertheim's perturbation theory,[29] was also combined with a number of quite simple mixing rules for the correlation of *PVTx* data; comparison of the results provided with those that arose from application of cubic EOS has enabled to select the most appropriate model for this strongly nonideal system.

Experimental Study

Materials and Sample Preparation. NMP (GC purity 99.9%) and methanol (GC purity 99.9%) were obtained from Fluka. They were stored in the absence of light over Fluka Union Carbide 0.4 nm molecular sieves to avoid moisture absorption, and were used without further purification. The pure solvents were degassed with ultrasound before the sample preparation. The binary liquid mixtures were prepared by syringing amounts, weighed to $\Delta m = \pm 1 \cdot 10^{-5}$ g with a Mettler AT 261 Delta Range balance, into suitably stoppered bottles. The mole fraction accuracy was estimated to be $\pm 1 \cdot 10^{-4}$.

Apparatus and Calibration Procedure. The schematic assembly of the apparatus is shown in Figure 1. The central element of the system, the Anton Paar DMA 512P high-pressure cell, was fit out with the stainless steel vibrating U-shaped tube as well as with the adequate electronics to excite the tube and measure the oscillating period. The Anton Paar DMA58 was used as a frequency counter joined to the high-pressure cell. A Julabo F32 circulating bath was in control of the cell temperature; the temperature was measured to ±0.01 K by using a calibrating Pt100 platinum sensor placed in the measuring cell, connected to a AΣΛ F250 unit. The circuit pressure was under the control of and measured by a Ruska 7615 digital pressure controller; the pressure was kept constant by the controller to ±0.005 MPa and was measured with a pressure sensor to ±0.01 MPa. The sample was separated from the pressurizing fluid by a high-pressure liquid-to-liquid separator (Pressurements T3600E), which was fit out with a Teflon diaphragm to forward the pressure. The pressure controller and the thermometer were previously calibrated through well-defined and traceable procedures. The whole system is computer controlled by a specially

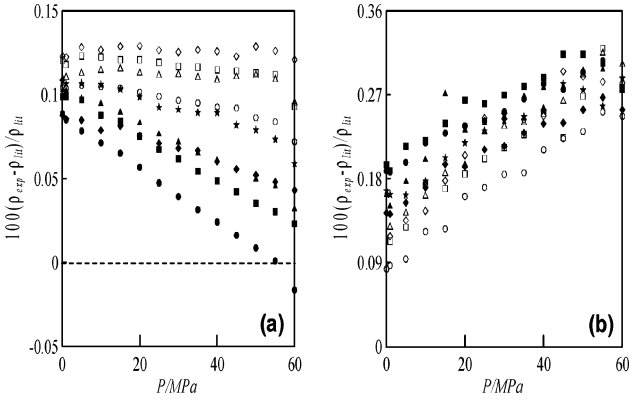

Figure 3. Relative deviations between the densities measured in this work and literature values for (a) NMP and (b) methanol. Literature values obtained from Ihmels and Gmehling (NMP)[8] and Reuck and Craven (Methanol).[30] (●) 278.15 K, (■) 288.15 K, (▲) 298.15 K, (◆) 308.15 K, (★) 318.15 K, (○) 328.15 K, (□) 338.15 K, (△) 348.15 K and (◇) 358.15 K.

developed software that allows fully automatic operation and makes the storage of a large number of accurate data feasible.

The calibration procedure to convert the densimeter oscillating period into density measurements was described in detail in a previous work.[19] A 14-parameter working equation was used whose parameters were obtained with water (Milli-Q, Millipore, resistivity 18.2 mΩ·cm) and *n*-hexane (Fluka, GC purity 99.9%) as standards. Aside from the uncertainties arising from pressure and temperature, the main source of experimental uncertainty regarding the density values stems from the two calibrating substances. Considering the full accuracies of all the contributing factors to the density readings, an accuracy ±0.0001 g cm^{-3} can be stated for the experimental densities.

Experimental Results. The densities of pure NMP and methanol, and of the x NMP + $(1 - x)$ methanol binary mixtures were measured in the compressed liquid state from 0.1 to 60 MPa (in 5 MPa steps) over the 278.15 to 358.15 K (in 10 K steps) temperature range. The density data for each composition were correlated with pressure and temperature using the TRIDEN 10-parameter equation,[4] which combines a modified Rackett equation for saturation densities with the Tait equation for isothermal compressed densities, eqs 1−3. In this work the value $P_0 = 0.1$ MPa was used as the reference pressure. The goodness of the fitting was evaluated through the absolute average percentage deviation (AAD) defined according to eq 4.

$$\rho_0 = \frac{A_R}{B_R^{[1+(1-T/C_R)D_R]}} \tag{1}$$

$$\rho = \frac{\rho_0}{1 - C_T \ln\frac{B_T + P}{B_T + P_0}} \tag{2}$$

$$B_T = b_0 + b_1\frac{T}{E_T} + b_2\left(\frac{T}{E_T}\right)^2 + b_3\left(\frac{T}{E_T}\right)^3 \tag{3}$$

$$\mathrm{AAD} = \frac{100}{N}\sum_{j=1}^{N}\left|\frac{\rho_{j,\mathrm{EXP}} - \rho_{j,\mathrm{CAL}}}{\rho_{j,\mathrm{EXP}}}\right| \tag{4}$$

The raw density data as a function of pressure and temperature are listed in the Supporting Information (Table 1), and the TRIDEN fitting coefficients are shown in Table 1. the fair

TABLE 1: Fitting Parameters of TRIDEN Correlation of Densities (g cm^{-3}) with Pressure and Temperature (eqs 1−3) and AAD Values (eq 4) for the x NMP + $(1 - x)$ Methanol Binary Solvent (parameters valid for 278.15−358.15 K and 0.1−60 MPa ranges)

parameter	$x = 0$	$x = 0.0972$	$x = 0.1963$	$x = 0.2933$	$x = 0.39393$	$x = 0.4910$	$x = 0.5986$	$x = 0.6985$	$x = 0.8049$	$x = 0.9024$	$x = 1$
C_T	0.092523	0.091397	0.088976	0.090001	0.084951	0.084796	0.085438	0.084516	0.084209	0.082513	0.089842
b_0(MPa)	224.0213	239.2738	251.1882	264.9089	266.8427	276.3058	281.5915	285.3978	294.4539	301.8009	336.899
b_1(MPa)	−35.2346	−20.0495	−7.9842	5.7167	9.9159	21.0254	27.7071	33.4448	40.4950	37.7468	7.9826
b_2(MPa)	−14.1326	−22.0883	−27.5784	−32.8699	−33.9727	−37.6285	−38.3576	−39.3464	−40.8414	−41.3272	−33.2787
b_3(MPa)	2.6384	3.5037	4.0220	4.4381	4.4793	4.7777	4.6434	4.6407	4.6768	4.8533	3.5926
E_T(K)	105.84	107.42	106.49	103.79	102.74	98.43	96.21	93.54	89.41	90.13	104.46
A_R (g cm^{-3})	34.2369	39.5977	49.2042	62.2182	75.4822	89.7966	106.1183	124.1742	139.4604	154.9861	30.4591
B_R	5.766365	6.052898	6.621939	7.342641	7.996536	8.646895	9.325390	10.025003	10.566022	11.091329	4.953406
C_R(K)	833.820	838.509	850.307	872.326	900.675	937.109	984.416	1042.125	1094.153	1149.330	838.680
D_R	−0.321502	−0.294980	−0.274579	−0.261635	−0.255427	−0.254345	−0.257431	−0.265137	−0.272480	−0.281249	−0.253190
AAD	0.0149	0.0124	0.0105	0.0089	0.0083	0.0074	0.0074	0.0067	0.0057	0.0058	0.0157

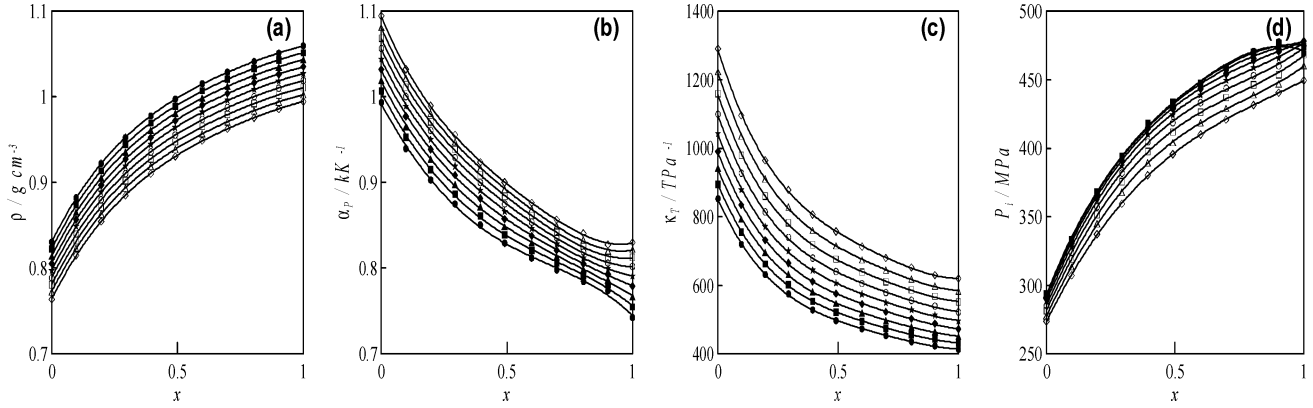

Figure 4. Temperature effect on the isobaric properties at $P = 30$ for the x NMP + $(1 - x)$ methanol binary solvents: (a) density, ρ; (b) isobaric thermal expansivity, α_P; (c) isothermal compressibility, κ_T; (d) internal pressure, P_i. Symbols as in Figure 3.

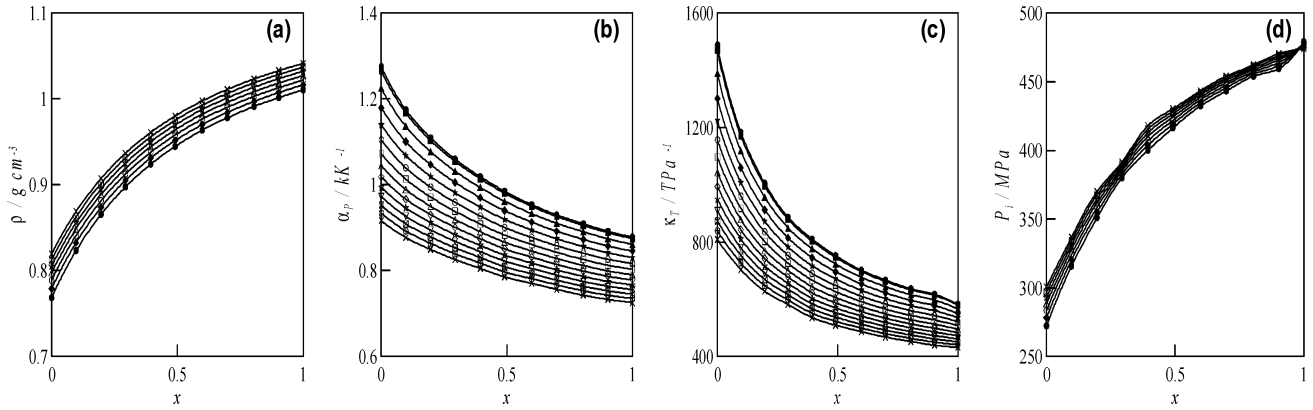

Figure 5. Pressure effect on the isothermal properties at $T = 318.15$ K for the x NMP + $(1 - x)$ methanol binary solvents: (a) density, ρ; (b) isobaric thermal expansivity, α_P; (c) isothermal compressibility, κ_T; (d) internal pressure, P_i. (●) 0.1 MPa, (■) 1 MPa, (▲) 5 MPa, (◆) 10 MPa, (★) 15 MPa, (○) 20 MPa, (□) 25 MPa, (△) 30 MPa, (◇) 35 MPa, (☆) 40 MPa, (▽) 45 MPa, (▼) 50 MPa, (⊕) 55 MPa and (×) 60 MPa.

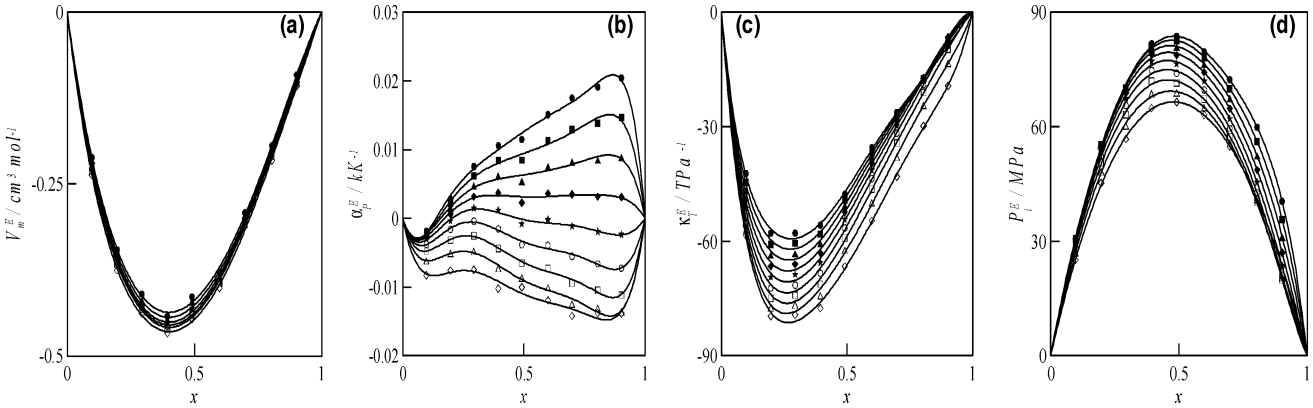

Figure 6. Temperature effect on the isobaric excess properties at $P = 30$ for the x NMP + $(1 - x)$ methanol binary solvents. (a) molar excess volume, V_m^E; (b) excess isobaric thermal expansivity, α_P^E; (c) excess isothermal compressibility, κ_T^E; (d) excess internal pressure, P_i^E. Symbols as in Figure 3.

agreement of the data measured with the literature values, 0.12% AAD for NMP and 0.32 AAD % for methanol, support the suitability of the apparatus for measuring densities of liquids under high-pressure conditions. Figure 2 plots both the experimental and fitted data for NMP and methanol, and Figure 3 shows the respective deviations with literature values.

From the experimental *PVTx* data, the isobaric thermal expansivity, α_P, isothermal compressibility, κ_T, and internal pressure, P_i, were calculated according to well-known thermodynamic expressions.[19] Figure 4 plots the temperature effect on the isobaric properties at the intermediate pressure 30 Mpa. Considering that the properties at the other pressures studied displayed the same trend, for reasons of simplicity only the data at 30 MPa are given. Figure 5 shows the pressure effect under isothermal conditions at 318.15 K (intermediate value across the studied range). A number of derived excess properties were determined from the measured and calculated properties, according to the critera by Benson and Kiyohara:[31] molar excess volumes, V_m^E, excess isobaric thermal expansivities, α_P^E, and excess isothermal compressibilities, κ_T^E. Evaluation of the non Gibbssian internal pressure[32] made it necessary to introduce an additional definition for its reference ideal value; therefore, the excess internal pressure, P_i^E, was calculated according to the definition put forward by Marczak.[33] The temperature effect on these excess properties at 30 MPa is plotted in Figure 6;

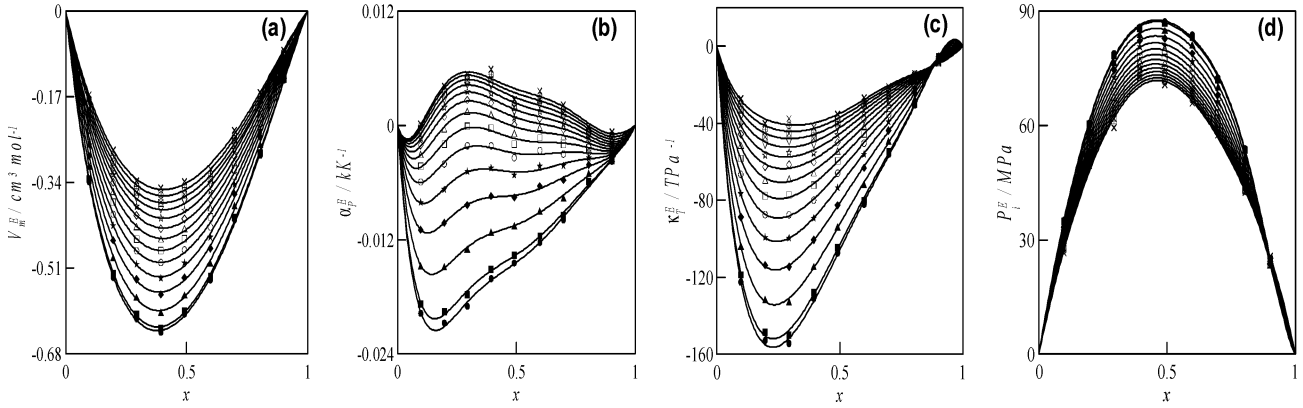

Figure 7. Pressure effect on the isothermal excess properties at $T = 318.15$ K for the x NMP + $(1 - x)$ methanol binary solvents: (a) molar excess volume, V_m^E; (b) excess isobaric thermal expansivity, α_P^E; (c) excess isothermal compressibility, κ_T^E; (d) excess internal pressure, P_i^E. Symbols as in Figure 5.

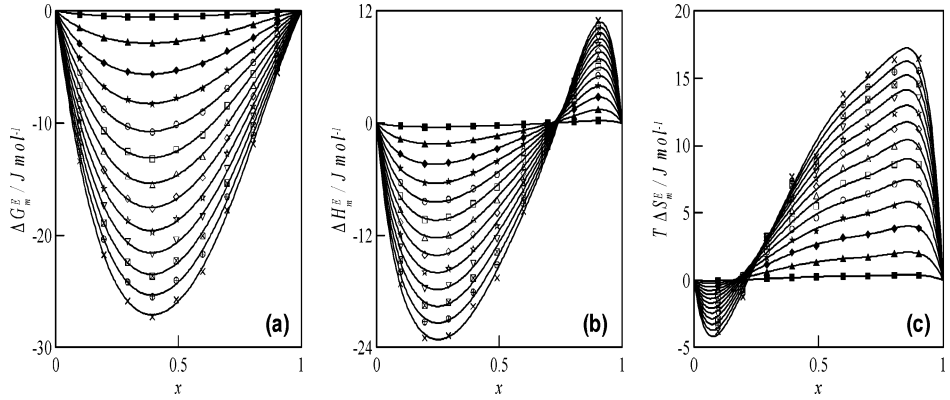

Figure 8. Pressure effect on the isothermal excess properties at $T = 298.15$ K relative to their values at 0.1 MPa for the x NMP + $(1 - x)$ methanol binary solvents: (a) excess Gibbs energy, ΔG_m^E; (b) excess enthalpy, ΔH_m^E; (c) temperature and excess entropy factor, $T \cdot \Delta S_m^E$. Symbols as in Figure 5.

Figure 7 shows the pressure effect at 318.15 K. The pressure effect on the isothermal excess Gibbs energy, ΔG_m^E, excess enthalpy, ΔH_m^E, and excess entropy, ΔS_m^E, were also calculated, taking 0.1 MPa and 298.15 K as reference values from known thermodynamic relations,[19] and are plotted in Figure 8.

Discussion. NMP is a rigid molecule devoid of specific interactions.[34] Although structural information (experimental or simulation studies) for pure NMP is lacking in the literature, so far the dipolar ordering appears to be the main controlling factor of the liquid structure. The abnormally high dipole moment[7,35] favors the formation of selective dipole−dipole self-associations, which result in the high dipolar ordering in the liquid-state reflected by the large density values (Figure 2a). The pyrrolidone group in NMP consists of both hydrophilic and hydrophobic moieties, which generate the significant structuring effect when mixing with water and related solvents such as methanol. Cross-association with these solvents is feasible through the two lone pair of electrons on the CO oxygen. On the contrary, the lone pair of electrons on nitrogen is sterically hindered; therefore, formation of H-bonding is unlikely.

The H-bonding structure of fluids such as methanol changes noticeably when the conditions are switched over from ambient to higher pressures and temperatures, or to the supercritical state. For decades the structure of pure methanol has attracted a great deal of attention. Although theoretical studies and calculations on the structure of liquid methanol have been extensively reported in the literature, so far the conclusions derived by different authors have been controversial, even using the same experimental techniques. Thus, molecular dynamics calculations,[36] Monte Carlo simulations,[37] ab initio,[38] and density functional[39] studies may be found in the literature. The structure of methanol has been studied also by experimental techniques such as neutron,[40,41] and X-ray[42] diffraction, and IR[43] and Raman[44] spectroscopies. The data analyses of pure methanol reveal that, as an average, typically each molecule is involved in only two or even less (∼1.8)[45] H-bonds; although a weakening is observed at high temperatures and pressures, NMP retains a certain H-bonding capability, even under supercritical conditions.[44] This notwithstanding, a strong controversy surrounding the nature of the clusters formed in pure methanol still remains. The early assumption of cyclic structures has been both supported and refuted by experimental and simulation studies, but an extended interpretation considers the formation of winding chainlike structures. In a recent paper, Guo et al.[46] have reported an X-ray emission spectroscopy study clearly showing that both rings and chains are concurrently present in liquid methanol, each made up of either 6 and/or 8 methanol molecules. However, at high pressures and temperatures, and under supercritical conditions, the average number of H-bonds drops to 1.6 per methanol molecule and the average chain-length to 3.1 molecules.[41]

Although the NMP/methanol system behaves strongly nonideally (Figures 4−8), deviations from the ideal behavior limit are less remarkable than those for NMP/water.[19] The values deduced for the excess properties can, in principle, be attributed to (i) differences in molecular interactions between like−like and unlike molecules, (ii) difference in shape and size of the components, and (iii) reorientation of the mixture molecules. The proton acceptor character of the amide oxygen in NMP may produce H-bonding NMP-methanol cross-associations upon

mixing; hence, heteroassociations should play quite an important role in the structuring of the mixed solvent. The H-bonding complexes formed are structured most likely as 1:2 NMP/methanol, because the two lone pair of electrons on the NMP CO oxygen may be H-bonded concurrently with two methanol molecules, giving rise to a strong structure.

The molar excess volumes deduced were negative throughout the full composition range over the pressure and temperature ranges studied and displayed only a small asymmetry. The minima observed in the alcohol-rich region (Figures 6a, 7a) support the formation of 1:2 NMP/methanol heteroassociations; that is, the lactam−methanol cross-association makes up for the disruption of the pure alcohol structure and the lactam dipolar ordering after mixing. Yet another noticeable effect arises from the difference in size and shape of the components; the variations in the free volume upon mixing, brought about by the fitting of the small alcohol molecules into the NMP voids, give rise to negative contributions to the molar excess volume. These features are supported by the other properties plotted in Figures 6 and 7. An increase in temperature is accompanied by a more negative molar excess volume, an effect brought about by the more efficient free volume effect the higher the temperature. This temperature effect, however, is less pronounced at the highest working pressures, indicating that the steric factors become less important at high pressures.

The excess enthalpy of the NMP/methanol system is strongly negative;[47] the minimum value $H_m^E = -660$ J mol^{-1} at $x = 0.5$ denotes that the NMP-methanol heteroassociations become partly balanced by the endothermic contributions arising from the disruptions of the alcohol and NMP structures, giving rise to a global exothermic mixing process. The pressure effect on the excess Gibbs energy, excess enthalpy, and excess entropy at constant temperature is somewhat more complex. An increase in pressure gives rise to a negative excess Gibbs energy contribution that can be attributed to the shape effect (Figure 8a). The pressure effect on the excess enthalpy changed from the alcohol-rich to the NMP-rich zones (Figure 8b). In the methanol-rich region, an increase in pressure gives rise to a more negative contribution, that is, to a more exothermic mixing ascribable to the larger effect of the cross-association contribution in this region, where the geometry effects by molecular fitting are less pronounced. In the NMP-rich region the main energetic effect stems from the disruption of the alcohol structure, not fully made up for by the new heteroassociations at such diluted methanol concentrations. The pressure effect on the excess entropy (Figure 8c) is also complex; at low NMP concentrations an increase in pressure gives rise to a (small) negative contribution brought about by the formation of the NMP−methanol complexes and the subsequent better ordered structure. However, when the NMP concentration increases, the geometrical fitting of methanol into the NMP structure is not sufficient to make up for the entropy increase caused by the disruption of the methanol structure.

EOS Study

Cubic EOS. The *PVTx* data of the pure and mixed solvents were correlated with the cubic EOS put forward by Soave (SRK),[22] Peng−Robinson (PR),[23] Peng−Robinson−Styjek−Vera (PRSV),[24] Patel−Teja (PT),[25] and Sako−Wu−Prausnitz (SWP)[26] combined with a number of mixing rules. A detailed description of the EOS used and the calculation procedures may be found in a previous paper.[19] The properties needed of the pure components required are listed in Table 2. The additional SWP parameters of the pure components (d and α_0) were evaluated from the correlation of the saturated NMP and methanol liquid densities; the saturated NMP liquid properties were reported earlier,[19] and those for methanol were obtained from Smith and Srivastava (1986).[51]

TABLE 2: Pure Component Parameters Required for the Application of Cubic EOS

	critical properties and acentric factor			SWP parameters[d]	
compound	P_C(MPa)	T_C(K)	ω	d	α_0
NMP	4.52[a]	721.8[a]	0.356[c]	0.1823	1.9161
methanol	8.09[b]	512.6[b]	0.556[b]	0.2009	4.5638

[a] Reference 48. [b] Reference 49. [c] Reference 50. [d] Parameters obtained with saturated liquid density correlation.

TABLE 3: AAD Values for the Correlation of *PVT* Data of Pure Solvents

	AAD (ρ^{LIQ})	
EOS	NMP	methanol
SRK	23.74	25.37
PR	15.02	12.84
PRSV	6.37	3.05
PT	14.19	11.42
SWP	0.08	1.99

TABLE 4: Mixing Rule Parameters, (eqs 5−16) and AAD Values Obtained with the SWP Equation for the Correlation of Compressed Liquid Density of NMP + Methanol Binary Solvent between 278.15−358.15 K and 0.1−60 MPa

mixing rule	k_{ij}	k_{ji}	m_{ji}	s_{ij}	l_{ij}	AAD (ρ^{LIQ})
quadratic	0.2417				0.0541	0.69
Panagiotopoulos	0.1886	0.4450			0.0637	0.62
Adachi	0.3168		0.1282		0.0637	0.62
Sandoval	0.7014	0.1886			0.0637	0.62
Schwartzentrüber	0.2417		0.1000	0.1000	0.0541	0.69
Stryjek	0.2553	0.5129			0.0683	0.63
Mathias	0.9284	3.4885			−0.0668	2.79

To a first stage, we have applied the five EOS for the prediction of *PVT* behavior of pure solvents. The AAD values for the two components and the five EOS are listed in Table 3. The predictions with SRK, PR, PRSV, and PT were rather inaccurate, and thus none of these equations represented well either the amount or the pressure and temperature dependence of the density values. The SWP EOS yielded lowest deviations and the most accurate prediction of the *PVT* behavior of the two pure solvents. Although the deviations for methanol were greater, SWP appears to be the only adequate cubic EOS for this system; therefore, SWP was the only EOS applied to the NMP + methanol binary solvent. To properly determine the EOS parameters, application of SWP requires use of suitable mixing rules. In this work, the van der Waals one-fluid mixing rules also with quadratic dependence for the b and c parameters were considered, eqs 5−7,

$$a = \sum_i \sum_j x_i x_j a_{ij} \tag{5}$$

$$b = \sum_i \sum_j x_i x_j b_{ij} \tag{6}$$

$$c = \sum_i \sum_j x_i x_j c_{ij} \tag{7}$$

except for the Mathias−Klotz−Praustnitz[52] mixing rule in a. The selected combining rules for the cross-terms are the classical quadratic one, eq 8, and those by Panagiotopoulos−Reid,[53] eq

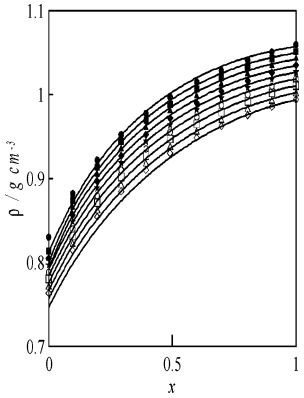

Figure 9. Experimental compressed liquid densities, ρ, at $P = 30$ for the x NMP + $(1 - x)$ methanol binary solvents. Symbols as in Figure 3 and (—) SWP correlation with the quadratic mixing rule.

9, Adachi−Sugie,[54] eq 10, Sandoval,[55] eq 11, Schwartzentrüber,[56] eq 12, Stryjek−Vera,[24] eq 13, and Mathias−Klotz−Prausnitz,[52] eq 14.

$$a_{ij} = (a_i a_j)^{1/2}(1 - k_{ij}) \tag{8}$$

$$a_{ij} = (a_i a_j)^{1/2}(1 - k_{ij}^{PR} + (k_{ij}^{PR} - k_{ji}^{PR})x_i) \tag{9}$$

$$a_{ij} = (a_i a_j)^{1/2}(1 - k_{ij}^{AS} - m_{ij}^{AS}(x_i - x_j)) \tag{10}$$

$$a_{ij} = (a_i a_j)^{1/2}(1 - k_{ij}^{SD} x_i - k_{ji}^{SD} x_j - 0.5(k_{ij}^{SD} + k_{ji}^{SD}) \times (1 - x_i - x_j)) \tag{11}$$

$$a_{ij} = (a_i a_j)^{1/2}\left(1 - k_{ij}{}^{S} - s_{ij}^{S}\frac{m_{ij}^{S} x_i - m_{ji}^{S} x_j}{m_{ij}^{S} x_i + m_{ji}^{S} x_j}\right) \tag{12}$$

$$a_{ij} = (a_i a_j)^{1/2}\left(1 - \frac{k_{ij}^{SV} k_{ji}^{SV}}{x_i k_{ij}^{SV} + x_j k_{ji}^{SV}}\right) \tag{13}$$

$$a = \sum_i \sum_j x_i x_j (a_i a_j)^{1/2}(1 - k_{ij}^{MKP}) + \sum_i x_i \left(\sum_j x_i ((a_i a_j)^{1/2} m_{ij}^{MKP})^{1/3}\right)^3 \tag{14}$$

For the b and c parameters, the cross coefficients were always obtained from eqs 15−16:

$$b_{ij} = \frac{1}{2}(b_i + b_j)(1 - l_{ij}) \tag{15}$$

$$c_{ij} = \frac{1}{2}(c_i + c_j)(1 - l_{ij}) \tag{16}$$

The results obtained from the correlation of the *PVTx* data using the SWP EOS combined with seven mixing rules are reported in Table 4. The goodness of the correlation was almost independent of the mixing rule selected; therefore, accurate enough results can be deduced with the simple two-parameter quadratic rule without introducing more complex mixing rules (Figure 9). For purposes of comparison, the TRIDEN correlation previously reported required 10 parameters for each composition. Although the AAD values provided were lower, the number of parameters was too high; therefore, with the simple SWP approach relatively accurate results can be obtained.

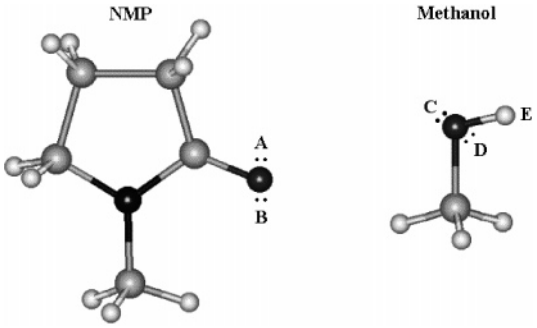

Figure 10. Association sites in NMP and methanol for the SAFT model.

The SAFT Model. The above cubic EOS are variations of the van der Waals equations; they are based on a hard-sphere reference term that describes the repulsive intermolecular interactions as a mean-field term for dispersion and other long-range forces.[57] This approach is not fully adequate for complex fluids such as those studied in this work. A more realistic reference term should include both the molecular shape and the intermolecular association, as well as some other interactions introduced as perturbation terms. The reference fluid may be described according to Wertheim's cluster expansion theory.[29] The SAFT theory[58] is a molecularly based equation of state that develops that approach using rigorous statistical mechanics. In the SAFT EOS, the component molecules are described as chains of segments and the residual Helmholtz energy is regarded as the sum of a main reference contribution and a minor dispersive perturbation. The reference term includes the hard-sphere, chain, and association terms, according to eq 17.

$$a = a^{ref} + a^{disp} = a^{hs} + a^{chain} + a^{assoc} + a^{disp} \tag{17}$$

In this work, the SAFT version developed by Huang and Radosz[27,28] was applied to describe the *PVT* behavior of both the pure components and the mixed solvent. The algebraic expressions for the model may be found in the original papers[27,28] and for reasons of simplicity are left out. The SAFT application requires knowledge of three pure component parameters for nonassociating fluids and five parameters for associating fluids, that is, the number of hard-sphere segments in each molecule, m, the segment volume, v^{00}, and the segment−segment interaction energy, u^0/k. The two additional parameters that account for the H-bonding interactions are the energy, ϵ/k, and the association volume, κ. The pure component parameters were regressed starting from the experimental saturated vapor pressure (NMP)[19] and the saturated liquid density data (methanol)[51] published earlier. The SAFT modeling for an associating fluid requires previous assignment of the association sites and the site−site interactions; therefore, in the SAFT interaction scheme applied for the NMP−methanol system, pure NMP was regarded as a nonassociating molecule (Figure 10) and methanol as an associative molecule with three associating sites (C, D, and E; Figure 10), the interaction energies between these sites being defined according to eqs 18−19.

$$\epsilon_{CC} = \epsilon_{DD} = \epsilon_{EE} = \epsilon_{CD} = 0 \tag{18}$$

$$\epsilon_{CE} = \epsilon_{DE} \neq 0 \tag{19}$$

Table 5 lists the model parameters deduced from the correlation of the saturation properties and AAD values, and Figure 11 shows the reasonably good fittings obtained for the

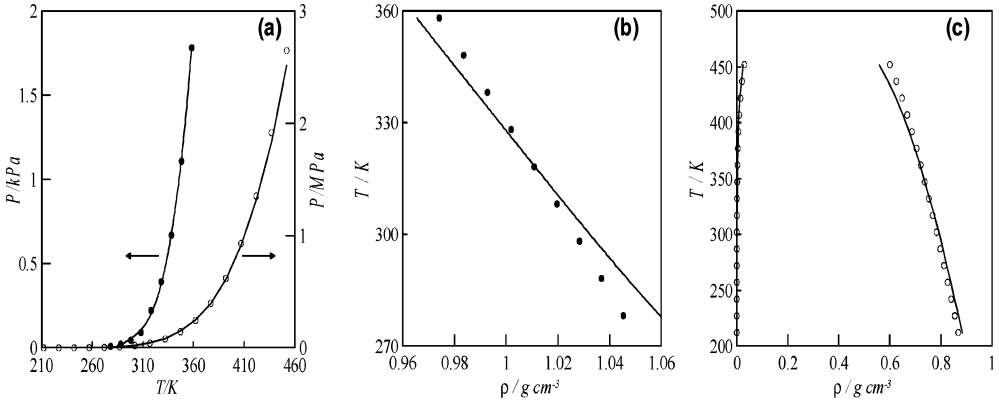

Figure 11. (a) Saturated pressure data, (b) saturated liquid density data for NMP, and (c) saturated vapor and liquid density data for methanol. (●) Experimental data from García et al. for NMP[19] and (○) from Smith and Srivastava for methanol,[51] and (—) SAFT model with parameters in Table 5.

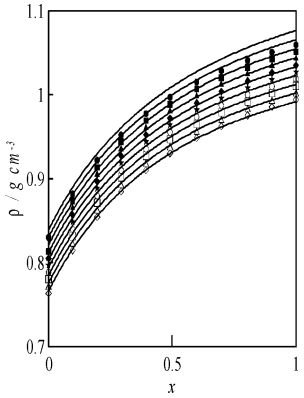

Figure 12. Experimental compressed liquid densities, ρ, at $P = 30$ for the x NMP + $(1 - x)$ methanol binary solvents. Symbols as in Figure 3 and (—) SAFT correlation with mixing rule I.

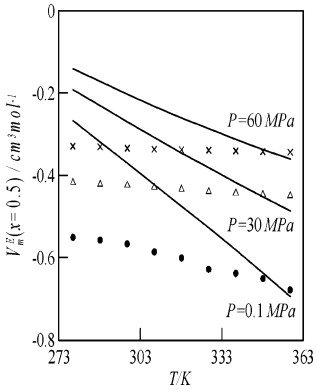

Figure 13. Experimental equimolar molar excess volumes, V_m^E ($x = 0.5$), for the x NMP + $(1 - x)$ methanol binary solvents. Symbols as in Figure 5 and (—) SAFT correlation with mixing rule I.

two components. The association parameters for methanol[59] can be used to evaluate the H-bonding enthalpy, $-\Delta H_H = 17.21$ kJ mol^{-1}, and entropy, $-\Delta S_H = 26.81$ J mol^{-1} K^{-1}, which were in good agreement with the experimental literature value, $-\Delta H_H = 16.7$ kJ mol^{-1}, [60] and give away the proper physical meaning of the SAFT parameters deduced.

Although pure NMP is regarded and modeled as a nonassociating molecule, when it is mixed with methanol the two lone pairs of electrons at the CO oxygen are prone to forming hydrogen bonds with the alcohol proton, giving rise to cross-association effects; hence, in the mixture two heteroassociation terms appear whose energies are defined according to eq 20.

$$\epsilon_{AE} = \epsilon_{BE} \neq 0 \tag{20}$$

Combination of EOS with adequate mixing rules plays a key role in the correlation performance of these models. Thus, several mixing rules were used for the correct application of the SAFT model to the NMP + methanol mixture. The cross-association energy, ϵ_{AE}, and volume, κ_{AE}, were obtained from correlation of the experimental *PVTx* data. The other parameters were also obtained from the same correlation together with the following mixing rules:[61] (mixing rule I) eqs 21, 22, 24, 26,

TABLE 5: SAFT Parameters and AAD Values for the Correlation of Saturation Properties of Pure Solvents

							AAD	
compound	T range (K)	v^{00} (mL mol^{-1})	m	μ^0/k(K)	ϵ/k(K)	$10^2\,\kappa$	P^{SAT}	$\rho^{SAT\,LIQ}$
NMP	278−358	11.66	4.568	305.51	−	−	0.44	5.76
methanol	212−452	13.05	1.700	304.97	2069.3	3.9780	3.00	1.96

TABLE 6: SAFT Parameters and AAD Values for the Correlation of *PVTx* Properties with the Different Mixing Rules for the x NMP + $(1 - x)$ Methanol Binary Solvent

mixing rule	λ_{12}	ξ_{12}	ϵ_{AE}/k (K)	$10^2\,\kappa_{AE}$	$-\Delta H_H$ (kJ mol^{-1})	$-\Delta S_H$ (kJ mol^{-1})	AAD (ρ^{LIQ})	AAD (V_m^E)
I	−0.0024	−	1170.8	2.7580	9.73	29.85	0.66	24.08
II	−0.0106	−	1040.0	2.1954	8.65	31.75	0.72	17.70
III	−0.0083	0.0009	1190.9	2.5415	9.90	30.53	0.69	19.62
IV	−0.0072	0.0009	1181.8	2.4012	8.96	29.31	0.62	18.25

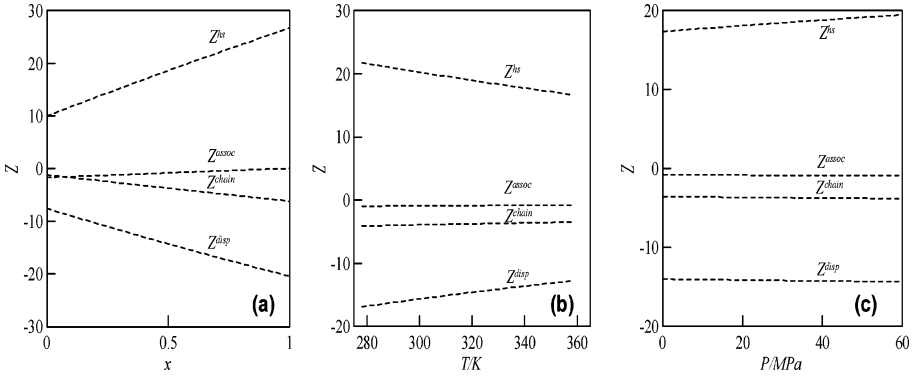

Figure 14. SAFT contributions to the total compressibility factor for the x NMP + $(1 - x)$ methanol binary solvents. (a) $P = 30$ and $T = 318.15$ K, (b) $x = 0.5$ and $P = 30$ MPa, and (c) $x = 0.5$ and $T = 318.15$ K.

and 27; (mixing rule II) eqs 21, 22, 25, 27, and 28; (mixing rule III) eqs 21, 23, 24, 26, and 27; (mixing rule IV) eqs 21, 23, 25, 27, and 28.

$$m = \sum_i \sum_j x_i x_j m_{ij} \tag{21}$$

$$m_{ij} = \frac{m_i + m_j}{2} \tag{22}$$

$$m_{ij} = \frac{m_i + m_j}{2}(1 - \xi_{ij}) \tag{23}$$

$$\frac{u}{kT} = \frac{\sum_i \sum_j x_i x_j m_i m_j \left(\frac{u_{ij}}{kT}\right) v_{ij}^0}{\sum_i \sum_j x_i x_j m_i m_j v_{ij}^0} \tag{24}$$

$$\frac{u}{kT} = \sum_i \sum_j f_i f_j \left(\frac{u_{ij}}{kT}\right) \tag{25}$$

$$v_{ij}^0 = \left[\frac{1}{2}((v_i^0)^{1/3} + (v_j^0)^{1/3})\right]^3 \tag{26}$$

$$u_{ij} = (u_{ii} u_{jj})^{1/2}(1 - \lambda_{ij}) \tag{27}$$

$$f_i = \frac{x_i m_i v_i^0}{\sum_j x_j m_j v_j^0} \tag{28}$$

To reach a more accurate representation of the derived excess properties, the density and molar excess volume values were correlated concurrently with the target function defined by eq 29:

$$F = \frac{100}{N}\sum_{j=1}^{N}\left|\frac{\rho_{j\mathrm{EXP}} - \rho_{j\mathrm{CAL}}}{\rho_{j,\mathrm{EXP}}}\right| + \frac{100}{N}\sum_{j=1}^{N}\left|\frac{V_{m,j\mathrm{EXP}}^{\mathrm{E}} - V_{m,j\mathrm{CAL}}^{\mathrm{E}}}{V_{m,j\mathrm{EXP}}^{\mathrm{E}}}\right| \tag{29}$$

Table 6 lists the parameters deduced from the correlation of the *PVTx* data for NMP−methanol and Figure 12 shows the experimental and correlated compressed liquid densities at 30 MPa and different temperatures. These data reveal good correlations for the density readings with only few parameters. The experimental and calculated equimolar molar excess volumes plotted in Figure 13 clearly indicate that the model provides less accurate values for excess properties. The correlations for molar excess volumes can be improved using the two-parameter mixing rules, but the density correlations are almost independent of the chosen mixing rule. In short, although the SAFT model appears to be adequate for this strongly nonideal system, to reach a better description of the excess properties use of somewhat more complex mixing rules is advisable.

Figure 14 plots the different contributions to the total compressibility factor. The hard-sphere and dispersive terms are the main contributing factors and operate in opposite sense. The associative contribution is important mainly at low NMP concentrations (Figure 14a) and it is almost constant with temperature and pressure (Figure 14b, 14c). This feature supports that H-bonding between NMP and methanol is a very important factor for the structure of this complex mixture, mainly at low lactam concentration.

Concluding Remarks

The strongly nonideal behavior of the NMP + methanol binary solvent was studied over wide ranges of pressure and temperature. From the measured and derived excess properties, strong H-bonding NMP−methanol interactions are inferred. The *PVTx* behavior was correlated with several cubic EOS, yielding inaccurate results with the most common EOS and very good data fitting with the Sako−Wu−Prausnitz equation. The SAFT model provided new parameters for the pure compounds and correlated fairly well the properties of the mixed solvent on the basis of a H-bonding interaction scheme. Although the correlation of the derived excess properties requires introduction of more complex mixing rules, accurate correlations can be obtained with this model.

Acknowledgment. The financial support by Junta de Castilla y León, Project BU10/03, and Ministerio de Educación y Ciencia, Project CTQ2005-06611/PPQ, (Spain) is gratefully acknowledged.

Supporting Information Available: Experimental densities of x *NMP* + $(1 - x)$ methanol as a function of pressure and temperature (Table 1). This material is available free of charge via the Internet at http://pubs.acs.org.

References and Notes

(1) Chen, C. C.; Mathias, P. M. *AIChE J.* **2002**, *48*, 194.
(2) Cox, K. R. *Fluid Phase Equilib.* **1993**, *82*, 15.
(3) Dohrn, R.; Pfohl, O. *Fluid Phase Equilib.* **2002**, *194*−*197*, 15.
(4) Ihmels, E. C.; Gmehling, J. *Ind. Eng. Chem. Res.* **2001**, *40*, 4470.
(5) Archer, W. L. In *Industrial Solvents Handbook*; Marcel Dekker: New York, 1996.

(6) Marcus, Y. In *The Properties of Solvents*; Wiley: Chichester, 1998.
(7) Lee, C. M.; Kumler, W. D. *J. Am. Chem. Soc.* **1961**, *83*, 4586.
(8) Ihmels, E. C.; Gmehling, J. *J. Chem. Eng. Data* **2002**, *47*, 1547.
(9) Hradetzky, G.; Hammerl, L.; Bittrich, H. J.; Wehner, K.; Kisan, W. In *Selective Solvents, Physical Sciences Data 31*; Elsevier: Amsterdam, 1989.
(10) (a) Gerster, J. A.; Gorton, J. A.; Eklund, R. B. *J. Chem. Eng. Data* **1960**, *5*, 423. (b) Wagner, U.; Weitz, H. M. *Ind. Eng. Chem*. **1970**, *62*, 43. (c) Ruiz, C.; Esteban, R.; Vega, A.; Diez, F. *Inst. Chem. Eng. Symp. Ser*. **1992**, *128*, B175. (d) Zheng, Y.; Chun, L.; Jin-Yuan, W. *Petrochem. Tech*. **2001**, *30*, 285. (e) Gaile, A. A.; Kostenko, A. V.; Zalischevskii, G. D.; Semenov, L. V.; Kaifadzhyan, E. A. *Chem. Technol. Fuels Oils* **2005**, *41*, 249.
(11) *N-Methyl-2-pyrrolidone Handbook*, Chemical Division, GAF, New York, 1972.
(12) Fischer, K.; Chen, J.; Petri, M.; Gmehling, J. *AIChE J*. **2002**, *48*, 887.
(13) Dyrkacz, G. *Energy Fuel* **2001**, *15*, 918.
(14) Prokopenko, N. A.; Bethea, I. A.; Clemens, C. J.; Klimek, A.; Wargo, K.; Spivey, C.; Waziri, K.; Grushow, A. *Phys. Chem. Chem. Phys.* **2002**, *4*, 490.
(15) Lawson, E. Q.; Sadler, A. J.; Harmatz, D.; Brandau, D. T.; Micanovic, R.; McElroy, R. D.; Middaugh, C. R. *J. Biol. Chem.* **1984**, *259*, 2910.
(16) García, B.; Alcalde, R.; Leal, J. M.; Matos, J. S. *J. Phys. Chem. B* **1997**, *101*, 7991.
(17) García, B.; Alcalde, R.; Aparicio, S.; Leal. J. M. *Phys. Chem. Chem. Phys*. **2002**, *4*, 1170.
(18) García, B.; Alcalde, R.; Aparicio, S.; Trenzado, J. L.; Leal, J. M. *Ind. Eng. Chem. Res*. **2003**, *42*, 920.
(19) García, B.; Alcalde, R.; Aparicio, S.; Dávila, M. J.; Leal, J. M. *Ind. Eng. Chem. Res.* **2004**, *43*, 3205.
(20) Sengers, J. V., Kayser, R. F., Peters, C. J., White, H. J., Eds. In *Equations of State for Fluids and Fluid Mixtures*; Elsevier: Amsterdam, 2000.
(21) Valderrama, J. O. *Ind. Eng. Chem. Res.* **2003**, *42*, 1603.
(22) Soave, G. *Chem. Eng. Sci*. **1972**, *27*, 1197.
(23) Peng, D.; Robinson, D. *Ind. Eng. Chem. Fundam.* **1976**, *15*, 59.
(24) Stryjek, R.; Vera, J. H. *Can. J. Chem. Eng*. **1986**, *64*, 334.
(25) Patel, N.; Teja, A. *Chem. Eng. Sci.* **1982**, *37*, 463.
(26) Sako, T.; Wu, A. H.; Prausnitz, J. M. *J. Appl. Polym.* **1989**, *38*, 1839.
(27) Huang, S. H.; Radosz, M. *Ind. Eng. Chem. Res.* **1991**, *30*, 1994.
(28) Huang, S. H.; Radosz, M. *Ind. Eng. Chem. Res.* **1990**, *29*, 2284.
(29) Wertheim, M. S. *J. Chem. Phys.* **1986**, *85*, 2929.
(30) Reuck, K. M.; Craven, R. J. B. In *Methanol. International Thermodynamic Tables of the Fluid State − 12*; Blackwell Science: Oxford, 1993.
(31) Benson, G. C.; Kiyohara, O. *J. Chem. Thermodyn*. **1979**, *11*, 1061.
(32) Reis, J. C. R.; Blandamer, M. J.; Davis, M. I.; Douhéret, G. *Phys. Chem. Chem. Phys.* **2001**, *3*, 1465.
(33) Marczak, W. *Phys. Chem. Chem. Phys.* **2002**, *4*, 1889.
(34) Dachwitz, E. *Ber. Bunsen-Ges. Phys. Chem*. **1987**, *91*, 1347.
(35) Fischer, E. *J. Chem. Soc*. **1955**, 1382.
(36) Guardia, E.; Martí, J.; Padro, J. A.; Saiz, L.; Komolkin, A. V. *J. Mol. Liq.* **2002**, *96*, 3.
(37) Shilov, I. V.; Rode, B. M.; Durov, V. A. *Chem. Phys.* **1999**, *241*, 75.
(38) Bako, I.; Palinkas, G. *J. Mol. Struct. (THEOCHEM)* **2002**, *294*, 179.
(39) Tsuchida, E.; Kanada, Y.; Tsukada, M. *Chem. Phys. Lett*. **1999**, *311*, 236.
(40) Yamaguchi, T.; Hidaka, K.; Soper, A. K. *Mol. Phys.* **1999**, *96*, 1159.
(41) Yamaguchi, T.; Benmore, C. J.; Soper, A. K. *J. Chem. Phys.* **2000**, *112*, 8976.
(42) Yamaguchi, T. *J. Mol. Liq.* **1998**, *78*, 43.
(43) Barlow, S. J.; Bondarenko, G. V.; Gorbaty, Y. E.; Yamaguchi, T.; Poliakoff, M. *J. Phys. Chem. A* **2002**, *106*, 10452.
(44) Ebukuro, T.; Takami, A.; Oshima, Y.; Koda, S. *J. Supercrit. Fluids* **1999**, *15*, 73.
(45) Dixit, S.; Crain, J.; Poon, W. C. K.; Finney, J. L.; Soper, A. K. *Nature* **2002**, *416*, 829.
(46) Guo, J. H.; Luo, Y.; Augustsson, A.; Kashtanov, S.; Rubensson, J. E.; Shuh, D. K.; Agren, H.; Nordgren, J. *Phys. Rev. Lett.* **2003**, *91*, 157401.
(47) López, E.; García, J.; Fernández, J. *J. Chem. Eng. Data* **1999**, *44*, 309.
(48) Gude, M. T.; Teja, A. S. *DIPPR Data Series*, **1994**, 174.
(49) Gude, M.; Teja. A. S. *J. Chem. Eng. Data* **1995**, *40*, 1025.
(50) Lide, D. R., Ed. *Handbook of Chemistry and Physics*, 82th ed.; CRC Press: Boca Raton, 2001.
(51) Smith, B. D.; Srivastava, R. In *Physical Sciences Data 25, Thermodynamic Data for Pure Compounds, Part B: Halogenated Hydrocarbons and Alcohols*; Elsevier: Amsterdam, 1986.
(52) Mathias, P. M.; Klotz, H. C.; Prausnitz, J. M. *Fluid Phase Equilibr*. **1991**, *67*, 31.
(53) Panagiotopoulos, A. Z.; Reid, R. C. *ACS Symp. Ser*. **1986**, *300*, 571.
(54) Adachi, Y.; Sugie, H. *Fluid Phase Equilibr*. **1986**, *28*, 103.
(55) Sandoval, R.; Wilczek-Vera, G.; Vera, J. H. *Fluid Phase Equilibr*. **1989**, *52*, 119.
(56) Schwartzentrüber, J.; Renon, H. *Fluid Phase Equilibr*. **1989**, *52*, 127.
(57) Müller, E. A.; Gubbins, K. E. *Ind. Eng. Chem. Res.* **2001**, *40*, 2193.
(58) Chapman, W. G.; Gubbins, K. E.; Jackson, G.; Radosz, M. *Ind. Eng. Chem. Res*. **1990**, *29*, 1709.
(59) Gupta, R. B.; Johnston, K. P. *Fluid Phase Equilibr*. **1994**, *99*, 135.
(60) Luck, W. A. P. In *Intermolecular Forces*; Springer: Heidelberg, 1991; Ch. 9.
(61) Zhong, C.; Yang, H. *Ind. Eng. Chem. Res.* **2001**, *41*, 4899.